Cell Reports
Medicine

Article

Single-cell RNA sequencing depicts the local cell landscape in thyroid-associated ophthalmopathy

Graphical abstract

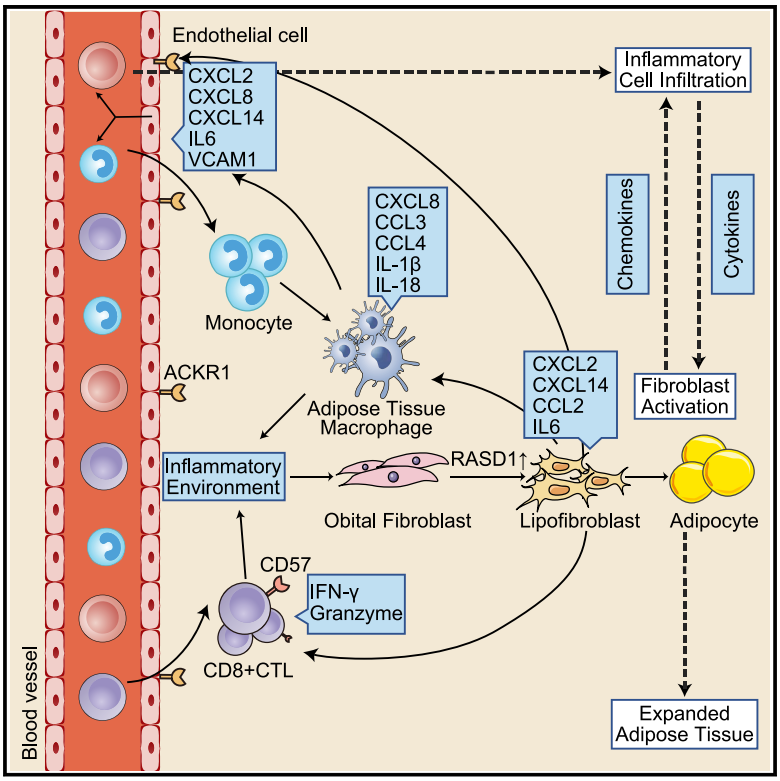

Highlights

- A local transcriptional landscape of orbital connective tissue in TAO is developed
- *RASD1*-expressing lipofibroblasts are highly involved in adipogenesis and inflammation
- *ACKR1*$^{+}$ endothelial cells contribute to inflammatory cell infiltration in TAO
- Adipose tissue macrophages engage in lipid metabolism and inflammatory response in TAO

Authors

Zhaohuai Li, Mei Wang, Jia Tan, ..., Rong Wang, Xianggui Wang, Wenru Su

Correspondence

wangxg@csu.edu.cn (X.W.), suwr3@mail.sysu.edu.cn (W.S.)

In brief

Thyroid-associated ophthalmopathy, characterized by orbital tissue expansion, remodeling, and fibrosis, commonly occurs in individuals with Graves' diseases and will threaten eyesight in its most severe form. Li et al. perform single-cell RNA sequencing in orbital tissues of individuals with TAO to identify transcriptional changes, which may serve therapeutic optimization.

Li et al., 2022, Cell Reports Medicine *3*, 100699
August 16, 2022
https://doi.org/10.1016/j.xcrm.2022.100699

CellPress

Cell Reports Medicine

CellPress
OPEN ACCESS

Article

Single-cell RNA sequencing depicts the local cell landscape in thyroid-associated ophthalmopathy

Zhaohuai Li,[1,6] Mei Wang,[2,6] Jia Tan,[3,4,6] Lei Zhu,[1,6] Peng Zeng,[2,6] Xiaozhen Chen,[5,6] Lihui Xie,[1] Runping Duan,[1] Binyao Chen,[1] Tianyu Tao,[1] Rong Wang,[1] Xianggui Wang,[3,4,*] and Wenru Su[1,7,*]

[1]State Key Laboratory of Ophthalmology, Zhongshan Ophthalmic Center, Sun Yat-sen University, Guangzhou 510060, China
[2]Department of Ophthalmology, Sun Yat-sen Memorial Hospital, Sun Yat-sen University, Guangzhou 510120, China
[3]Eye Center of Xiangya Hospital, Hunan Key Laboratory of Ophthalmology, Xiangya Hospital, Central South University, Changsha 410078, China
[4]National Clinical Research Center for Geriatric Disorders, Xiangya Hospital, Central South University, Changsha 410078, China
[5]Hunan Key Laboratory of Skin Cancer and Psoriasis, Xiangya Hospital, Central South University, Changsha 410008, China
[6]These authors contributed equally
[7]Lead contact
*Correspondence: wangxg@csu.edu.cn (X.W.), suwr3@mail.sysu.edu.cn (W.S.)
https://doi.org/10.1016/j.xcrm.2022.100699

SUMMARY

There is a specific reactivity and characteristic remodeling of the periocular tissue in thyroid-associated ophthalmopathy (TAO). However, local cell changes responsible for these pathological processes have not been sufficiently identified. Here, single-cell RNA sequencing is performed to characterize the transcriptional changes of cellular components in the orbital connective tissue in individuals with TAO. Our study shows that lipofibroblasts with *RASD1* expression are highly involved in inflammation and adipogenesis during TAO. *ACKR1*$^+$ endothelial cells and adipose tissue macrophages may engage in TAO pathogenesis. We find CD8$^+$CD57$^+$ cytotoxic T lymphocytes with the terminal differentiation phenotype to be another source of interferon-γ, a molecule actively engaging in TAO pathogenesis. Cell-cell communication analysis reveals increased activity of *CXCL8/ACKR1* and *TNFSF4/TNFRSF4* interactions in TAO. This study provides a comprehensive local cell landscape of TAO and may be valuable for future therapy investigation.

INTRODUCTION

Thyroid-associated ophthalmopathy (TAO) is an autoimmune condition affecting the orbit and ocular adnexa that may lead to orbital disfigurement, double vision, and even vision loss.[1] TAO is observed in about 2 in 10,000 individuals per year and has a prevalence of 25%–40% among individuals with Graves' disease. It induces negative health and economic consequences.[2] Treatment of TAO remains challenging because of a poor understanding of its pathogenesis.[3] Glucocorticoids are the mainstay treatment for reducing inflammation,[4] but they usually have a limited success rate and many side effects. Relapse occurs frequently after drug discontinuation.[5] Rehabilitative surgery is often required to solve the immediate risk to vision or restore normal orbital anatomy.[5] Understanding the pathogenesis of TAO will help improve the available treatment methods.

The main processes involved in TAO are inflammation, glycosaminoglycan accumulation, adipogenesis, and myofibrogenesis in the periocular tissue.[6] These changes lead to the pathologic changes characteristic of TAO: orbital tissue expansion, remodeling, and fibrosis.[1,7] Several cells have been reported to be responsible for these changes. Immune cells, especially T cells, infiltrate the orbital tissue; secrete cytokines such as interferon-γ (IFN-γ), interleukin-1β (IL-1β), and tumor necrosis factor alpha (TNF-α); and activate orbital fibroblasts.[8–10] Orbital fibroblasts (OFs) have long been regarded as target cells in TAO because of their ability to secrete abundant hyaluronan and differentiate into adipocytes and myofibroblasts (MYFs).[7,11] Activation of OFs through thyroid-stimulating hormone (TSH) receptor antibody (TRAb) suggests a link between TAO and Graves' disease.[12]

Current studies mainly focus on the role of CD4$^+$ T cells and OFs in TAO.[13,14] Whether other cell types are involved in TAO and the molecular regulation is largely unknown. Our study created comprehensive transcriptional atlases of the cellular components in the orbital connective tissue (OCT) from healthy controls (HCs) and individuals with TAO by single-cell RNA sequencing (scRNA-seq), a powerful tool to dissect the cellular heterogeneity and reveal complex cellular events. Our study revealed the pro-inflammation and pro-adipogenesis role of lipofibroblasts (LPFs) with ras-related dexamethasone-induced 1 (*RASD1*) expression. Atypical chemokine receptor 1 (ACKR1$^+$) endothelial cells (ECs) and adipose tissue macrophages (ATMs) with an M2 phenotype were also identified as playing a role in TAO. CD8$^+$CD57$^+$ cytotoxic T lymphocytes (CTLs) showed the terminal differentiation phenotype and high IFN-γ gene expression. This study may complement our current TAO knowledge and prompt development of novel therapeutic strategies.

RESULTS

Single-cell analysis and cell type identification

The transcriptome of OCT from HCs and individuals with TAO were determined through scRNA-seq. The clinical characteristics of these individuals are shown in Table S1. Single-cell suspensions were converted to barcoded scRNA-seq libraries using the 10X Genomics platform, and 31,353 cells were reserved for further analysis (Figure 1A). These cells were clustered into six cell types based on their canonical lineage markers: OFs (*CD34*$^+$ *PDGFRA*$^+$ *COL1A1*$^+$), natural killer (NK) and T cells (NK&TCs; *CD3E*$^+$), myeloid cells (MCs; *LYZ*$^+$), B cells (BCs; *CD79A*$^+$), ECs (*PECAM1*$^+$), and pericytes (PCs; *MCAM*$^+$ *RGS5*$^+$) (Figures 1B–1D). Adipocytes, with a marker of *ADIPOQ*,[15] were not detected in our data, possibly because of their easier rupture characteristic and larger size (Figures 1B–1D and S1A). OFs accounted for more than 80% of all cells in the OCT of HCs, with a small proportion of other cell types (Figure 1E). Increased NK&TCs and MCs were found in TAO. This suggests their possible pathogenic role (Figure 1E).

scRNA-seq revealed OF subsets with pathogenic properties in TAO

OFs have been identified as the core of TAO pathogenesis.[16,17] Previous studies commonly classified them into a *THY1*$^+$ (*CD90*$^+$) population with the potential to differentiate into MYFs and a *THY1*$^-$ population with the potential to differentiate into adipocytes.[18] In our study, OFs were classified into three subsets based on their expression of *THY1*, *RASD1*, and other functional genes (Figures 2A–2C). Differentially expressed genes (DEGs) of each subject are shown in Data S1. *THY1*$^+$ MYFs highly expressed matrix remodeling-related genes (*COL1A1*, *DCN*, *MMP2*, *COL12A1*, *CTHRC1*, and *POSTN*),[19,20] an inflammatory gene (*CXCL14*), and muscle contraction-related genes (*TAGLN* and *ACTA2*). *RASD1*$^+$ LPFs highly expressed inflammatory genes (*IL6*, *CCL2*, and *ICAM1*) and adipogenesis- or lipid accumulation-related genes (*RASD1*, *CEBPB*, *PPARG*, *PLIN2*, *PTGDS*, and *APOD*).[21,22] Conversely, *THY1*-*RASD1*-conventional OFs (COFs) expressed low levels of these genes (Figures 2B and 2C). Subsequent Gene Ontology (GO) analysis also showed enriched pathways related to adipogenesis and inflammation in LPFs, whereas MYFs highly expressed pathways related to matrix remodeling, muscle contraction, and inflammation (Figure 2D). The different gene signatures of these OF subtypes indicate their diverse functions.

During the TAO process, LPFs showed increased proportions (Figure 2E). We also conducted a pseudotime analysis to explore the relationships and possible transitions among the fibroblast subpopulations during TAO. This analysis showed a trajectory with two major branches (Figure 2F). COFs, MYFs, and LPFs equally constituted the state 1 branch, representing the initial states of fibroblasts. LPFs constituted most of the state 2 branch, representing the cellular states of the LPF phenotype (Figure 2F). MYFs and COFs constituted most of the state 3 branch, suggesting relatively similar phenotypes (Figure 2F). The trajectory dominated by TAO displayed a significant shift toward the LPF phenotype (Figure 2F). These results suggest that LPF differentiation and lipid expansion may be the major processes in OCT during TAO.

Next we explored the transcriptional changes of LPFs in TAO. We conducted a DEG analysis of LPFs between TAO and HCs (Figure 3A). In TAO, LPFs exhibited upregulated adipogenesis-related genes (*APOE*, CCAAT/enhancer-binding protein (C/EBP), β (*CEBPB*), *CEBPD*, *FABP4*, *FABP5*, *APOC1*, *RASD1*, and *PLIN2*), inflammation-related genes (*IL6*, *CXCL2*, *CCL2*, and *PTGDS*), and genes related to cell proliferation and activation (*JUNB*, *JUND*, *MYC*, and *PIM1*). *IGF1*, a growth factor, was also upregulated in LPFs in TAO (Figure 3A; Data S1). Corresponding upregulated pathways of LPFs were shown by GO analysis (Figure 3B). These upregulated genes of LPFs in TAO were similar to the genes highly expressed by LPFs compared with the other two OF subsets (Figures 3C and 3D). A Venn diagram identified 142 genes highly expressed by LPFs and upregulated in TAO as LPF-specific upregulated genes (Figures 3C and 3D). These genes were related to adipogenesis, cell activation, growth factors, and cytokines. (Figure 3D). *RASD1*, a gene reported to mediate adipogenesis and diet-induced obesity,[22] was mainly expressed by LPFs. It is also upregulated during TAO (Figure 3E). Expression of this gene was also positively correlated with the expression of three critical adipogenic transcription factors: *CEBPB*, *CEBPD*, and peroxisome proliferator-activated receptor γ (*PPARG*) (Figure S1B).[22,23] We also observed an upward trend of expression of adipogenesis-associated genes (*FABP4*, *FABP5*, *CEBPB*, *CEBPD*, *PLIN2*, *PPARG*, and *RASD1*) along the LPF differentiation path (Figure 3F). These results indicate that expression of *RASD1* might be a characteristic of fibroblasts with the tendency for adipocyte differentiation. Intriguingly, expression of *PIM1*, which is involved in a wide range of cancers,[24] showed a similar trend as the adipogenesis-associated genes, supporting their role in promoting the LPF phenotype of OFs in OCT (Figure 3F). Immunofluorescence confirmed enhanced *PIM1* expression in TAO (Figure 3G).

OCT underwent lipid expansion and inflammation in TAO, driven by LPFs. Our study indicates a potential role of *Pim1* in activation and differentiation of OFs in TAO.

scRNA-seq revealed the involvement of ACKR1$^+$ ECs in TAO pathogenesis

Stromal cells are a heterogeneous group of cells with essential functions in health and disease.[25] The OFs, ECs, and PCs identified in our OCT samples pertain to stromal cells.[26] According to the top 10 DEGs of each cell type, ECs highly expressed genes encoding chemokine or inflammatory molecules (such as *CCL14*) and genes related to antigen presentation (including *HLA-DRB1*, *HLA-DRA*, and *CD74*)[27] (Figure S1C). GO analysis showed that ECs were related to regulation of cell adhesion in addition to their role in angiogenesis. This suggests their potential pro-inflammatory function (Figure S1D). The top 10 DEGs (such as *DCN* and *FBLN1*) and enrichment pathways in OFs were related to extracellular structure organization. PCs highly expressed genes (such as *TAGLN* and *ACTA2*) and pathways related to muscle system regulation (Figures S1C and S1D). Their gene signatures indicated their distinct functions in vascular development, extracellular structure organization, and muscle system regulation. ECs exhibit pro-inflammatory potential and may engage in TAO pathogenesis.

We also identified two subclusters of ECs, and they could be distinguished by whether *ACKR1* was expressed (Figure 4A).

CellPress
OPEN ACCESS

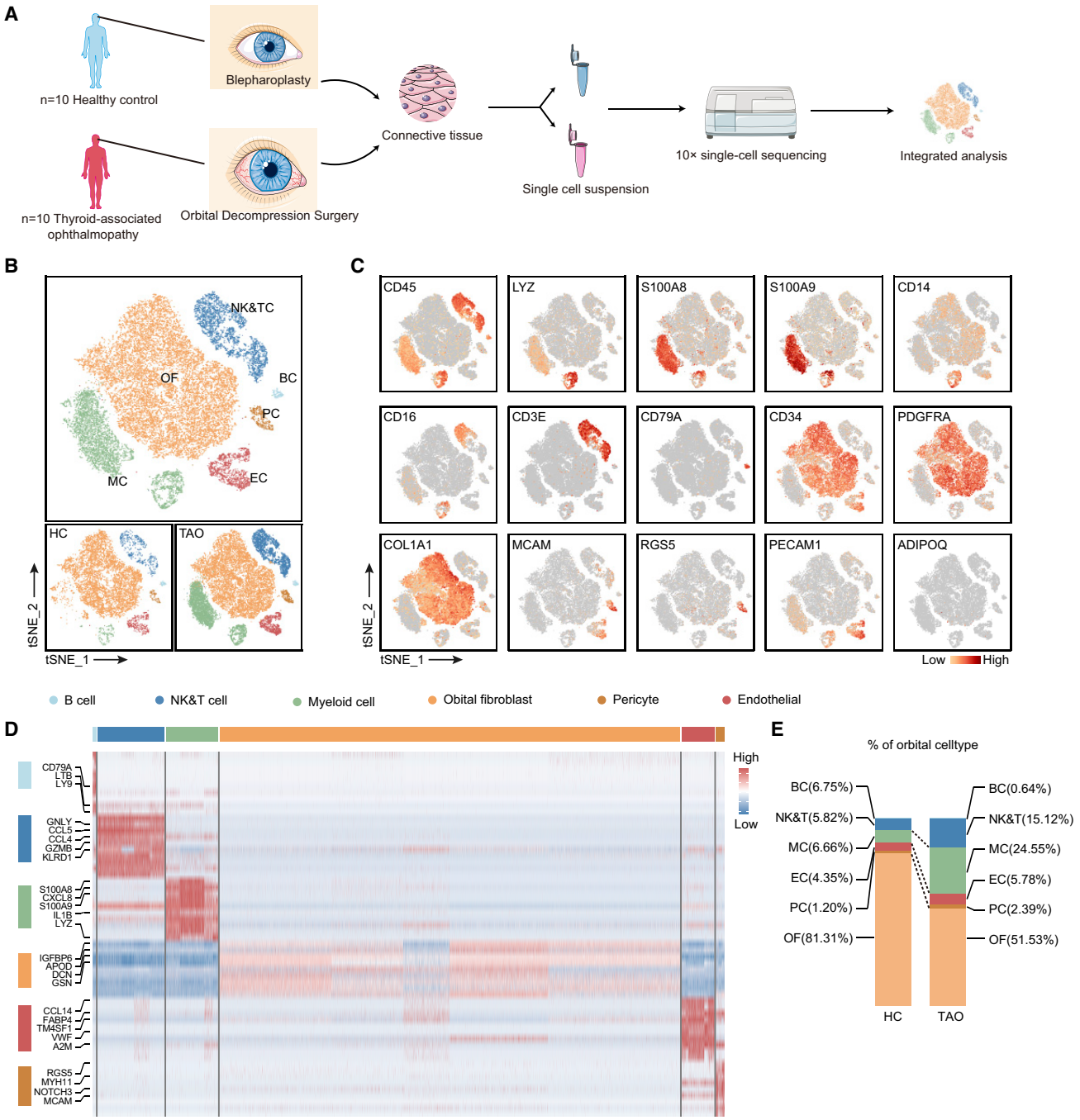

Figure 1. Study design and unbiased classification of cells

(A) Schematic of the experimental design for single-cell RNA sequencing (scRNA-seq). The orbital connective tissue (OCT) was isolated from healthy controls (HCs) and individuals with thyroid-associated ophthalmopathy (TAO) and subsequently processed through scRNA-seq using the 10X Genomics platform.

(B) t-SNE plot showing clusters of major cell types.

(C) t-SNE plots of canonical markers for major cell types in the OCT.

(D) Heatmap showing scaled expression of discriminative gene sets for major cell types in the OCT. The color scheme is based on *Z* score distribution from −2 (blue) to 2 (red).

(E) Bar chart showing the relative proportion of major cell types in OCT from HCs and individuals with TAO derived from scRNA-seq data.

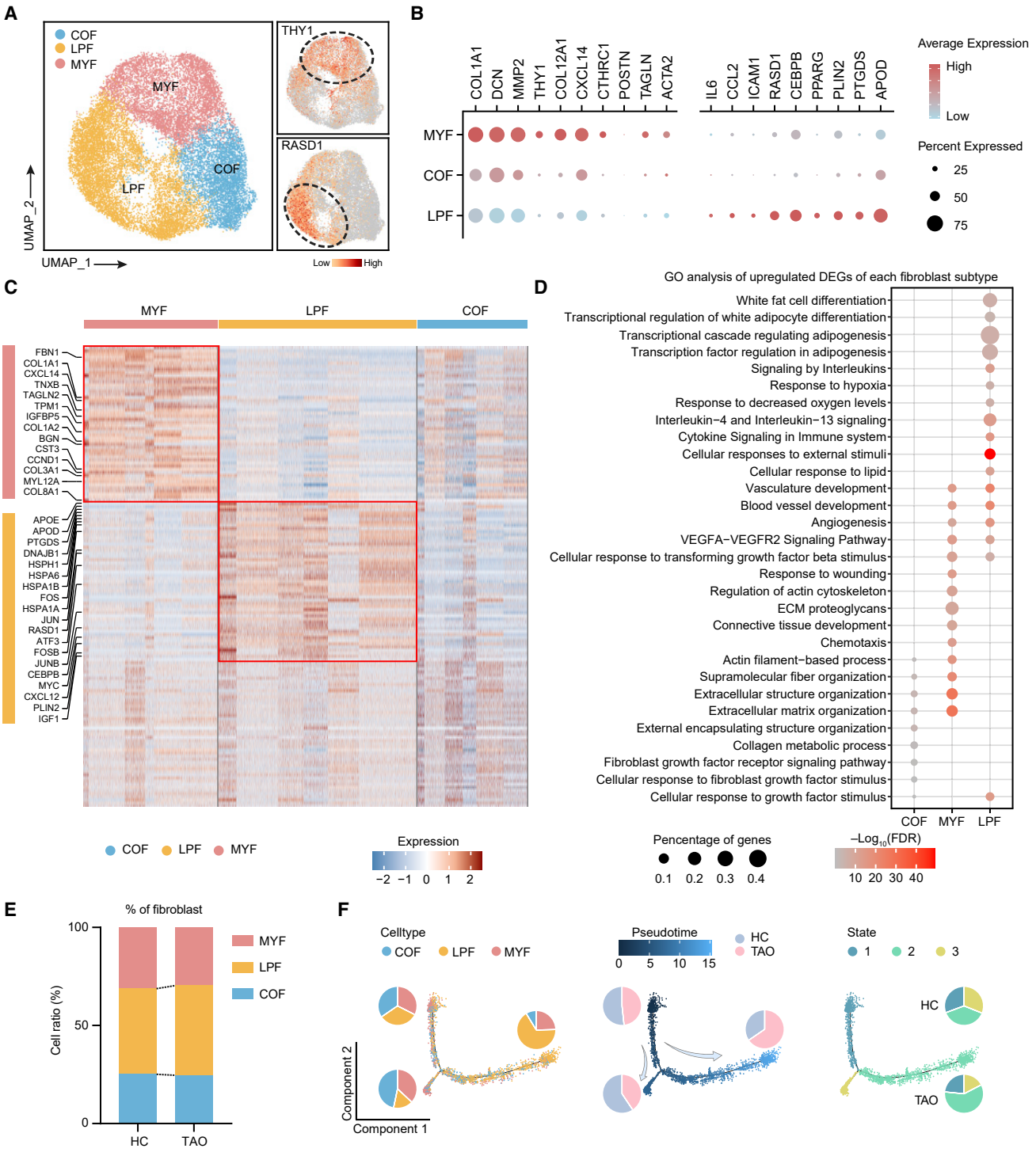

Figure 2. Characterization of OF subsets in OCT in TAO

(A) Uniform manifold approximation and projection (UMAP) plot showing clusters of orbital fibroblast (OF) subsets.

(B) The expression levels of selected functional genes in OF subsets.

(C) Heatmap showing scaled expression of discriminative gene sets in each OF subset. The color scheme is based on *Z* score distribution from −2 (blue) to 2 (red).

(D) Representative GO terms and KEGG pathway enriched by upregulated DEGs of each OF subset.

(E) Bar chart showing the relative proportion of each OF subset in OCT from HCs and individuals with TAO.

(F) Pseudotime analysis of OF subsets. Left: distribution of the three subpopulations on each of the branches. Center: distribution of the cells from HCs or individuals with TAO on each of the branches. Right: the relative proportion of cells in each state in HCs and individuals with TAO.

CellPress
OPEN ACCESS

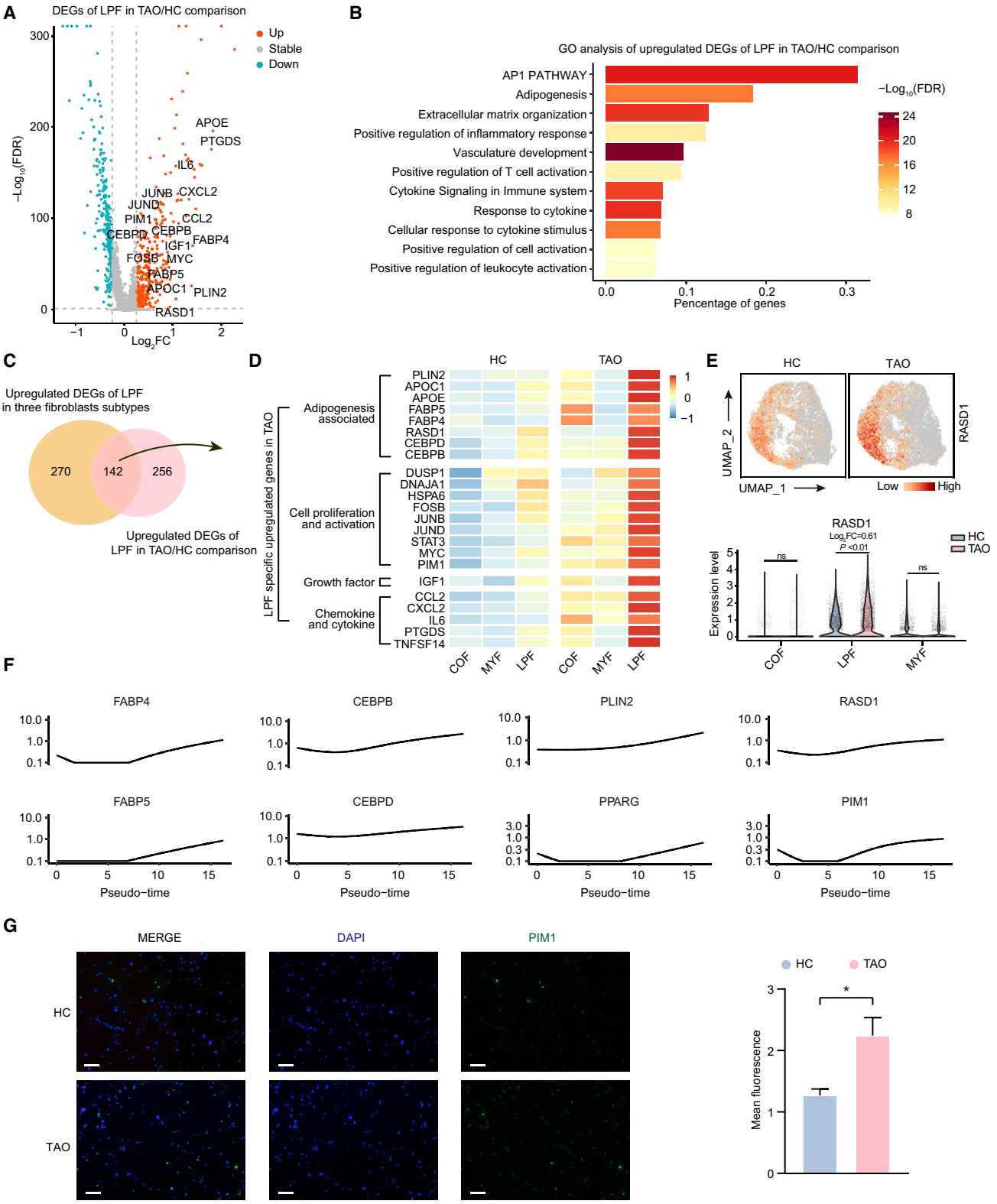

(legend on next page)

ACKR1 can bind to numerous C-X-C motif (CXC) and C-C motif (CC) chemokines with high affinity. It has been identified recently as a venular capillary marker.[28–30] As shown in Figure 4B, ACKR1$^+$ ECs highly expressed genes encoding cytokines, chemokines, and antigen-presenting molecules such as *IL6*, *CSF3*, *CCL14*, selectin E (*SELE*), and *HLA-DRA*, whereas ACKR1$^-$ ECs expressed high levels of genes involved in blood vessel or extracellular matrix structure, including *CLDN4*, *DST*, and *FN1* (Figure 4B; Data S1). Except for the blood vessel development pathway, ACKR1$^+$ ECs were highly involved in pathways related to angiogenesis, cytokine response, cell adhesion, inflammation, and antigen processing and presentation compared with ACKR1$^-$ ECs (Figure 4C). Therefore, expression of *ACKR1* may represent an EC phenotype actively engaging and responding to inflammatory cell infiltration into OCT.

We then explored their role in TAO pathogenesis. ACKR1$^-$ ECs outnumber ACKR1$^+$ ones during healthy states, and their proportion is reversed in TAO (Figure 4D). During TAO, ACKR1$^+$ ECs expressed higher levels of chemokines (*CXCL2*, *CXCL3*, *CXCL8*, *CXCL10*, and *CXCL14*), adhesion molecules (*SELE*, *SELP*, integrin subunit α V [*ITGAV*], and *VCAM1*), and inflammatory molecules (*CSF3*, *IL6*, and *IL1R1*). HIF1A, the master regulator of cellular adaptation to hypoxia, was also highly expressed by ACKR1$^+$ ECs in TAO.[31] ACKR1$^-$ ECs also expressed higher levels of chemokines and *IL6* (Figures 4E, 4G, and 4H; Data S1). Some of extracellular matrix structure genes (*COL3A1*, *COL1A1*, *FN1*, *VCAN*, and *LUM*) were upregulated in ACKR1$^-$ ECs (Figures 4F, 4G, and 4H; Data S1). Pathways associated with inflammation, cytokine signaling, cell adhesion, and vascular endothelial growth factor (*VEGF*) were upregulated more evidently in ACKR1$^+$ ECs during TAO, whereas ACKR1$^-$ ECs showed more evident upregulation in extracellular structure and matrix organization (Figure 4I).

These results suggest that ACKR1$^+$ ECs may be the EC subsets that more actively participate in TAO pathogenesis by mediating leukocyte movement and promoting inflammation.

Terminally differentiated CD8$^+$ TCs with the capacity to secrete IFN-γ are identified in TAO

TCs are one of the primary infiltrating immune cell types in the OCT of individuals with TAO (Figure 1E). We reclustered NK&TCs into five clusters: CD4$^+$ T memory (Tm) cells (*CD4*$^+$*GZMK*$^+$), CD8$^+$ Tm cells (*CD8A*$^+$ *GZMK*$^+$), CD8$^+$ CTLs (*CD8A*$^+$ *GZMB*$^+$), CD56 (*NCAM1*$^+$) CD16 (*FCGR3A*$^+$) NK2 cells (*NCR1*$^+$*FCGR3A*$^+$), and CD56$^+$CD16$^-$ NK1 cells (*NCR1*$^+$*NCAM1*$^+$*FCGR3A*$^-$) (Figures 5A, 5B, and S1E; Data S1). IFN-γ plays an important role in TAO with its ability to induce production of multiple chemoattractants and glycosaminoglycan by OFs.[6] It is conventionally identified as a T helper (Th) type 1 cell cytokine in TAO.[32,33] We evaluated the expression of *IFNG* in TC subsets and observed that it was mainly expressed by CD4$^+$ Tm and CD8$^+$ CTL cells. CD4$^+$ Tm cells highly expressed *CCR7* and the TC exhaustion marker *PDCD1* (Figure 5C).[34] CD8$^+$ CTL cells highly expressed a chemokine receptor (*CX3CR1*), terminal differentiation markers (including B3GAT1 [coding CD57] and *KLRG1*),[35,36] and cytotoxicity-related genes (including *PRF1* and *GNLY*) (Figure 5C). Therefore, as two sources of *IFNG*, CD4$^+$ Tm cells may tend to be exhausted, whereas CD8$^+$ CTLs showed the terminal differentiation phenotype (*B3GAT1*$^+$*KLRG1*$^+$) in OCT. A previous study had reported that CD57 staining was detected in OCT in TAO.[37] Although CD57$^+$CD8$^+$ TC express only low levels of most chemokine receptors (CCR7 and CXCR4), they display up-regulation of CX3CR1, which induces migration of CD8 TCs to peripheral tissues.[38]

We next explored the functional changes of TC subsets in TAO by conducting DEG and GO analysis. During TAO, CD4$^+$ Tm cells expressed higher levels of chemokines and chemokine receptors (*CXCL8*, *CCL8*, *CCR6*, and *CCR7*) as well as cytokine receptors (*IL7R*, *IL4R*, and *CCL20*). Cell activation-related genes (*FOSB*, *JUNB*, *JUN*, and *FOS*) and co-stimulatory molecules (*CD27*, *CD28*, and *CD40LG*) were downregulated in CD4$^+$ Tm cells, indicating an activation deficiency of these cells (Figure 5D; Data S1). In CD8$^+$ CTL cells, chemokine and chemokine receptors, cytotoxicity-related genes (*GZMK* and *GZMM*), and IFN signaling-related genes (such as *ISG20*, *IFITM1*, and *IFITM2*) were upregulated (Figure 5E; Data S1). CD8$^+$ Tm, NK1, and NK2 cells also showed various degrees of upregulation of expression of chemokines and IFN signaling-related genes (Figure S1F; Data·S2). Subsequent GO analysis of the upregulated DEGs of TC subsets during TAO also exhibited upregulation in pathways related to IFN signaling, immune or inflammatory response, cytokine signaling, and cell killing, most prominently in CD8$^+$ CTLs (Figure 5F). These findings suggest that CD8$^+$ CTLs with the terminal differentiation phenotype may also actively engage in *IFNG* expression, immune cell recruitment, cell killing, and inflammatory response in TAO except from CD4$^+$ Th cells.

ATMs are a pathogenic cell type involved in TAO

Four mononuclear phagocytic cell subtypes were identified in our data: CD16$^+$ monocytes (Mos; *FCGR3A*$^+$), CD14$^+$ Mos (*CD14*$^+$*S100A8*$^+$*S100A9*$^+$), dendritic cells (DCs; *CD1C*$^+$), and macrophage (Macs; *MARCO*$^+$) (Figures 6A, 6B, and S2A; Data·S2). Pseudotime analysis showed that Mos evolved into DCs and Macs in OCT tissue (Figure S2B). We also identified neutrophils in OCT from individuals with TAO based on expression of *CSF3R*,

Figure 3. Characterization of LPF subsets in OCT in TAO

(A) Volcano plot showing DEGs of LPF subsets in TAO/HC comparison.

(B) Venn diagram showing comparative analysis of upregulated DEGs of LPF subsets in three fibroblast subtypes and upregulated DEGs of LPF subsets in TAO/HC comparison. The count shows the number of DEGs.

(C) Heatmap of the relative expression of selected LPF-specific upregulated DEGs in HC and TAO groups in different fibroblast subtypes.

(D) Bar chart showing representative GO terms and KEGG pathways enriched in upregulated DEGs of LPF subtypes in TAO/HC comparison.

(E) UMAP plot showing the expression of ACKR1 and CXCR2 of OCT cells from HCs and individuals with TAO.

(F) Pseudotime-ordered single-cell expression trajectories for FABP4, FABP5, CEBPB, CEBPD, PLIN2, PPARG, RASD1, and PIM1.

(G) Representative images of immunostaining of cross-sections of OCTs from HCs and individuals with TAO for PIM1 (green) and nuclei (4′,6-diamidino-2-phenylindole [DAPI]; blue).

Each group contains six samples. Data are represented as mean ± SEM. Significance was determined using unpaired Student's t test. *$p < 0.05$.

CellPress
OPEN ACCESS

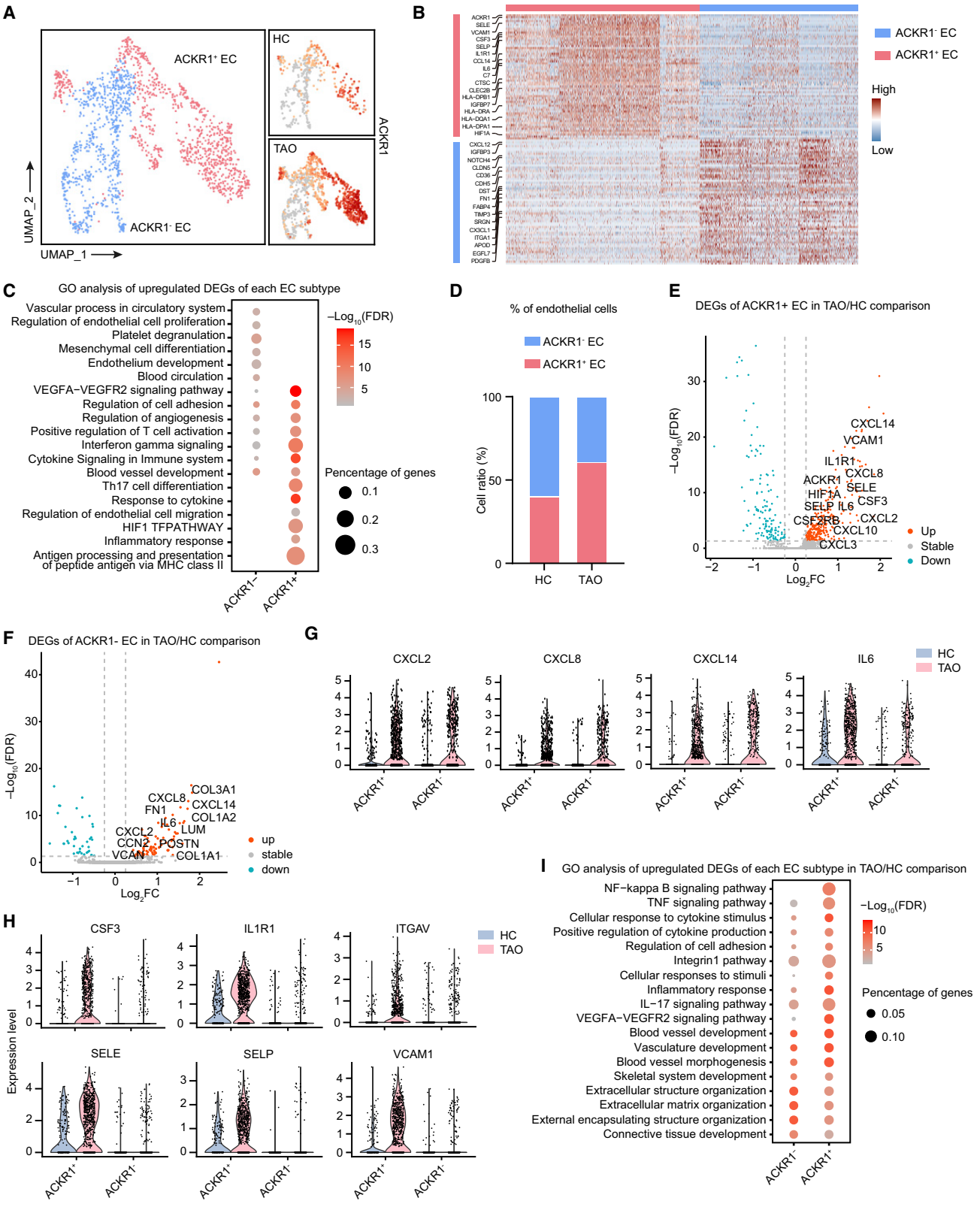

(legend on next page)

FCGR3B, and upregulated genes compared with other cell types in OCT (Figures S2C and S2D), which were not found in HCs. These neutrophils highly expressed genes involved in neutrophil degranulation and activation, and neutrophil-mediated immunity compared with other cell types in OCT (Figure S2E).

In TAO, Mo infiltration into the OCT was mostly attributed to classic CD14$^+$ Mos with critical pro-inflammatory function (Figure S2F).[39] We also explored the functional changes of the four cell types in TAO by conducting DEG and GO analyses. CD16$^+$ Mos exhibited upregulated pathways related to cytokine signaling harboring DE-Gs, including *IFNGR1*, *IL1R2*, *TNFSF13*, and *IL2RG* (Figures 6C and S2H; Data·S2). In CD14$^+$ Mos, some inflammatory genes were upregulated, including *S100A9*, *S100A8*, *S100A12*, *CSF3R*, and *NLRP3*, consistent with their previously identified pro-inflammatory role[39] (Figure 6D; Data·S2). Cytokine signaling (including IL- and IFN-γ-related) was also highly upregulated in CD14$^+$ Mos (Figure S2H). DCs also showed upregulated pathways related to inflammatory response and cytokine signaling harboring DEGs, such as *S100A9*, *NLRP3*, *IFNGR2*, and *CXCR4* Figures 6E and S2H; Data·S2). In Macs, in addition to chemokines and cytokines, genes related to lipid metabolism (such as *CEBPB*, *APOE*, and *FABP5*) were also upregulated. In contrast, genes related to antigen presentation (such as *HLA-DMA* and *CD74*), the immune negative regulator *CD200R*,[40] and genes inhibiting complement activation (*CD55* and *CD52*) were downregulated in Macs in TAO (Figure 6F; Data·S2). It has been reported that ATMs participate in lipid metabolism in the steady state but contribute to adipose tissue inflammatory response under pathologic conditions.[41] However, their status and function have not been described in TAO. Our data showed that, in the OCT, which consists mainly of adipose tissue, Macs highly expressed *CD36*, a scavenger receptor facilitating fatty acid transport,[42] and *CD163* and *MRC1*, two markers of M2-like Macs[43] from both study groups (Figure 6G). It is interesting that ATMs in our data exhibited an M2 phenotype, an anti-inflammatory phenotype, but expressed high levels of inflammatory genes during TAO. Subsequent GO analysis also identified upregulated pathways related to lipid metabolism (annotated as long-chain fatty acid transport, the PPAR signaling pathway, and cellular response to lipid), cytokine signaling (including IFN-γ and IL-18 signaling), and inflammatory response (Figure 6H).

Therefore, in OCT of individuals with TAO, ATMs exhibit an M2 phenotype but retain inflammation-promoting capacity and may engage in lipid metabolism in the microenvironment of OCT.

Constructing an OF-based regulatory network for TAO

Next we explored the cell-cell communication network using CellphoneDB2. MYFs and LPFs showed enhanced interactions with ACKR1$^+$ ECs in TAO compared with healthy states (Figures 7A and 7B). Considering the central role of OFs in TAO, we developed a pathogenic OF-based interaction network (Figures S3 and S4). Immune cells were found to express elevated cytokines, including *IL6*, *TNFA*, *TGFB*, and *IFNG*, acting on pathogenic OFs, that secreted chemoattractants to promote lymphocyte infiltration into OCT. This finding was consistent with previous reports[44,45] (Figures S3 and S4). The interactions of IL-6/IL-6 receptor, transforming growth factor β (TGF-β)/TGF-β receptor, and chemokines/chemokine receptors were enhanced during TAO, suggesting that these pairs may enhance the interaction of immune cells and pathogenic OFs. Considering the potent interaction between ACKR1$^+$ ECs and OFs in TAO (Figure 7A), we next explored the ligand-receptor pairs associated with ACKR1$^+$ ECs and OFs. Our study found that OFs produced VEGF, which acted on ECs, and, conversely, that ECs produced platelet-derived growth factor (PDGF) to promote OF proliferation in TAO (Figure 7B). The interactions of chemokines (including *CXCL8*, *CXCL1*, and *CCL2*) and *ACKR1* between OFs and ACKR1$^+$ ECs were enhanced in TAO (Figure 7B). The elevated interaction of *CXCL8* and *ACKR1* between Macs and ECs has been identified in skin diseases, and this interaction is co-opted to recruit immune cells to inflammatory sites.[46] We also detected increased *CXCL8* expression in nearly all cell types in OCT from individuals with TAO, and this molecule actively interacted with *ACKR1* on ACKR1$^+$ ECs in TAO (Figures 7C and 7D). These results again indicated that ACKR1$^+$ ECs highly engaged in leukocyte recruitment into OCT in TAO and that the *CXCL8/ACKR1* interaction may contribute to this recruitment process. We observed that the interaction of *TNFSF4* (OX40L) and *TNFRSF4* (OX40),[47] a pair of TC co-stimulatory molecules, between MYFs and immune cells was overactive in TAO (Figure 7E). *TNFSF4* and *TNFRSF4* work cooperatively to regulate TC biology, and their interactions prompt TC to exhibit the effector memory phenotype but reduce their regulatory function.[47,48] *TNFSF4* has been reported to be expressed by MYFs in fibrotic skin, promoting fibrosis by recruiting CD4$^+$ TC, which actively secrete pro-inflammatory mediators and activate fibroblasts.[49] The cell-cell communication network analysis identified MYFs as the major source of *TNFSF4* and acting on CD4$^+$ Tm cells (Figures 7E and 7F). Thus, the OX40L/OX40 interaction between MYFs and TCs might participate in the higher OCT inflammation and fibrosis in TAO.

DISCUSSION

scRNA-seq is an unbiased global technology for analyzing cells from tissue and peripheral blood.[50,51] We developed a

Figure 4. Characterization of EC subsets in OCT in TAO

(A) UMAP plot showing clusters of endothelial cell (EC) subsets.

(B) Heatmap showing scaled expression of discriminative gene sets for ACKR1$^+$ and ACKR1$^-$ ECs in OCT. The color scheme is based on *Z* score distribution from −2 (blue) to 2 (red).

(C) Bar chart showing the relative proportion of ACKR1$^+$ and ACKR1$^-$ ECs in OCT from HCs and individuals with TAO.

(D) Representative GO terms and KEGG pathway enriched by upregulated DEGs of each EC subtype.

(E and F) Volcano plots showing DEGs of ACKR1$^+$ EC (E) and ACKR1$^-$ EC (F) subsets in TAO/HC comparison.

(G) Violin plot showing the expression of CXCL2, CXCL8, CXCL14, and IL-6 in ACKR1$^+$ ECs and ACKR1$^-$ ECs from HCs and individuals with TAO.

(H) Violin plot showing the expression of CXCL2, CSF3, IL-1R1, ITGAV, SELE, SELP, and VCAM1 in ACKR1$^+$ ECs and ACKR1$^-$ ECs from HCs and individuals with TAO.

(I) Representative GO terms and KEGG pathway enriched by upregulated DEGs of ACKR1$^+$ ECs and ACKR1$^-$ ECs in TAO/HC comparison.

CellPress
OPEN ACCESS

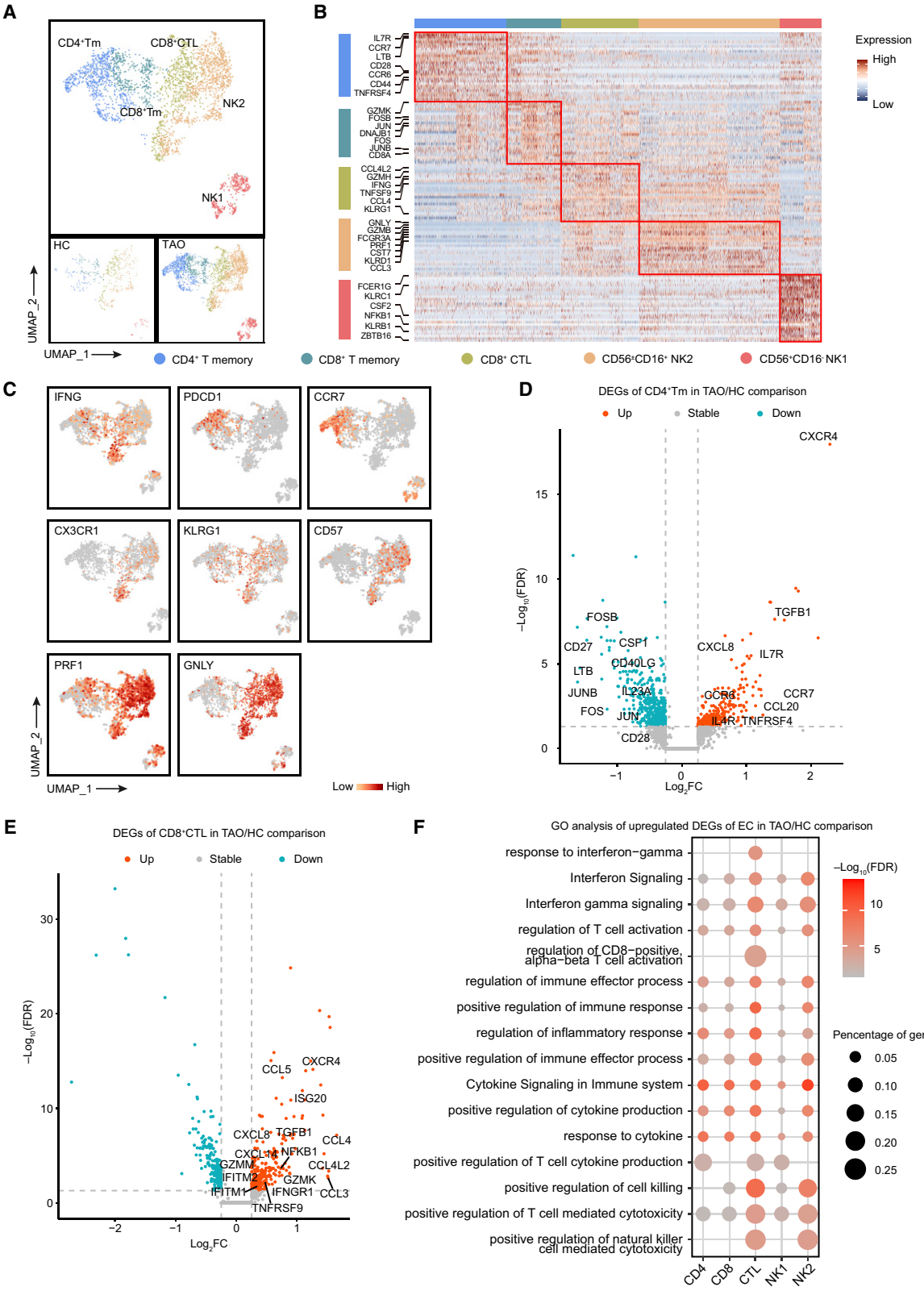

(legend on next page)

comprehensive transcriptional atlas of OCT in both study groups and revealed cellular components in the OCT in TAO pathogenesis. We identified six major cell types and 17 cell subsets that showed distinct properties in TAO. ECs were also involved in TAO pathogenesis, among which ACKR1$^+$ ECs might be an EC subset actively mediating leukocyte trafficking. We also highlighted that terminally differentiated CD8$^+$ CTL cells might be a sustained INF-γ resource and contribute to persistent inflammation. We identified ATM participation in inflammation and lipid metabolism in TAO. The cellular components in OCT constitute an OF-based regulatory network that engages in TAO pathogenesis.

OFs have been identified as central cells in TAO with the ability to proliferate, secrete hyaluronan, and differentiate into MYFs or adipocytes.[16] These induce characteristic eye muscle enlargement and orbital fat expansion in TAO.[16,17] Koumas et al.[52] divided OFs into two subsets based on *THY1* (*CD90*) glycoprotein expression. *THY1*$^-$ OFs have a strong ability to differentiate into adipocytes, whereas *THY1*$^+$ OFs may differentiate into MYFs. In our study, three OF subsets were identified based on expression of *THY1* and other functional genes. *THY1*$^+$ MYFs showed gene signatures similar to the previously reported *THY1*$^+$ OFs. These cells highly expressed genes involved in extracellular matrix organization and muscle contraction. The LPFs and COFs identified in our study showed low or undetectable *THY1* expression, and only *RASD1*$^+$ LPFs exhibited potent adipogenesis and pro-inflammation capacity, as indicated by DEG and GO analysis. *RASD1* is essential for adipogenesis and diet-induced obesity.[22] Without *RASD1*, mitotic clonal expansion and adipocyte differentiation is abolished.[22,23] Three critical adipogenic transcription factors (*CEBPB*, *CEBPD*, and *PPARG*)[22,23] have been reported to be positively regulated by *RASD1*. In our study, *RASD1* was mainly expressed by LPFs, and its expression was positively correlated with *CEBPB*, *CEBPD*, and *PPARG*. Therefore, high expression of *RASD1* might characterize adipocyte differentiation in OFs. In TAO, expression of *RASD1* and a series of adipogenesis-associated genes was increased in LPFs, indicating active adipogenesis in OCT. *PIM1*, an oncogene widely known for its proliferative effects,[53] was upregulated along LPF differentiation path. A previous study has identified *PIM1* as a differentiation marker in adipocytic neoplasm.[54] Our study suggested that *PIM1* may promote differentiation of into pathogenic LPFs, serving as a target for TAO.

The regulatory role of ECs in inflammation has been reviewed elsewhere[55] but has not been identified in TAO. We observed that ECs also contributed to inflammation promotion according to their gene signatures. The vascular system consists of segments with different functions, and, in most cases, leukocyte adhesion and emigration are mediated by postcapillary venules and collecting venules.[56] Resting ECs do not interact with leukocytes.[57] However, during inflammation, activated ECs express adhesion molecules or chemokines to induce leukocyte recruitment.[55] *ACKR1* has been identified recently as a vascular capillary marker.[30] In our study, ACKR1$^+$ ECs exhibited upregulated genes and pathways related to cell adhesion and migration compared with ACKR1$^-$ ECs. In TAO, pathways related to cytokine stimulation, inflammatory response, and regulation of cell adhesion were upregulated in ACKR1$^+$ ECs. These results suggest that the ACKR1$^+$ ECs in our study might be postcapillary or collecting venous cells with the ability to recruit leukocytes into the OCT in TAO.

Previous studies have paid much attention to the role of TCs, especially CD4$^+$ TCs, in TAO.[58] It is commonly accepted that Th1 cells secreting IL-1β, IL-2, TNF-α, and IFN-γ are activated in the initial phase of TAO, whereas Th2 cells activate and secrete IL-4, IL-5, IL-10, and IL-13 in the late phase.[59,60] Compared with CD4$^+$ TCs, the role of CD8$^+$ TCs in the disease process has not been sufficiently identified. In adipose tissue from mice fed a high-fat diet, CD8$^+$ effector TCs have been reported to outnumber CD4 TCs and have a role in recruiting Macs, promoting local inflammation.[61] In OCT containing adipose tissue, our study also identified the important role and special phenotype of CD8 TCs. CD8$^+$ CTL cells in the OCT exhibited a terminal differentiation phenotype, potent cytotoxicity, and IFN-γ secretion capacity. Accumulation of these CD57$^+$ TCs has been observed in natural human aging and various diseases associated with chronic immune activation.[35,62] Our study identifies involvement of these terminally differentiated CD8$^+$ CTL cells in the pathogenesis of TAO. IFN-γ induces production of multiple chemoattractants and glycosaminoglycan by OFs.[6] These cells may be another source of INF-γ during the disease process, apart from Th1 cells. Another study identified a group of CD4$^+$ cytotoxic TCs with chemotactic and inflammatory features that are specific to TAO.[63] However, the CD4$^+$ TCs identified in our study did not show cytotoxicity markers but exhaustion markers. Terminally differentiated TCs have been reported to exhibit reduced proliferation capacity,[62] high cytotoxicity, and reserved IFN-γ secretion capacity.[38,64] In contrast, exhausted T cells may experience functional loss and reduced IFN-γ production.[65,66] Our study indicates that CD4$^+$ TCs tend to be exhausted and that their IFN-γ production may be reduced, whereas CD8$^+$ TCs tend to be terminally differentiated and continuously secrete IFN-γ as the disease course is prolonged.

Among Macs, various phenotypes and functions of ATMs have been widely discussed in the context of obesity.[67] In expanded adipose tissue, infiltration of Macs is an important physiological phenomenon, and these Macs cooperate with adipocytes to regulate the inflammatory response.[68] Hypoxia and chemokines are two factors that promote Mac recruitment in

Figure 5. Characterization of NK&TC subsets in OCT in TAO

(A) UMAP plot showing clusters of NK&TC subsets.

(B) Heatmap showing scaled expression of discriminative gene sets for NK&TC subsets in OCT. The color scheme is based on *Z* score distribution from −2 (blue) to 2 (red).

(C) UMAP plot showing the expression of selected genes in NK&TC subsets.

(D and E) Volcano plots showing DEGs of CD4$^+$ Tm cell (D) and CD8$^+$ CTL (E) subsets in TAO/HC comparison.

(F) Representative GO terms and KEGG pathway enriched by upregulated DEGs of each NK&TC subtype in OCT in TAO/HC comparison.

CellPress
OPEN ACCESS

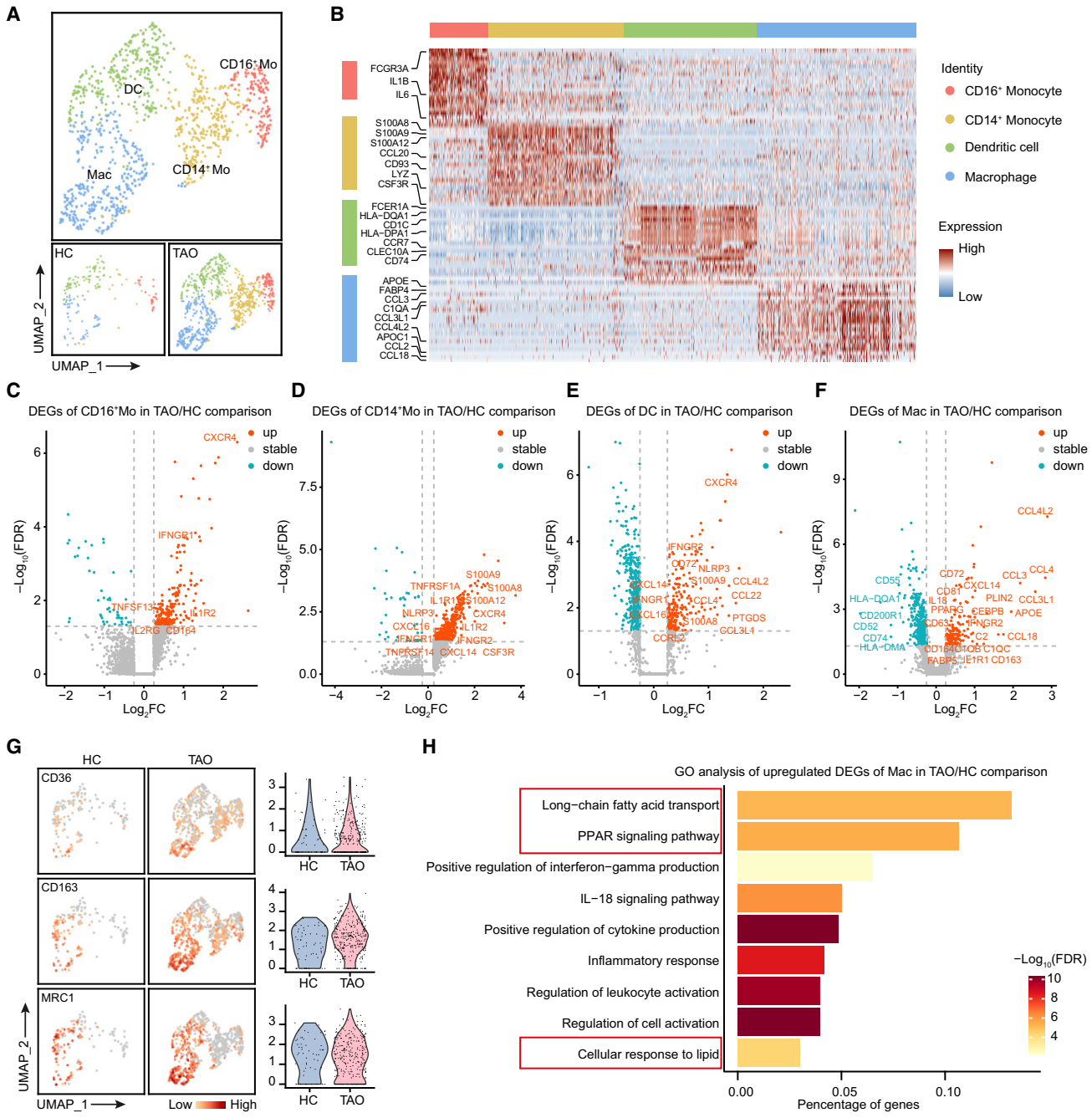

Figure 6. Characterization of MC subsets in OCT in TAO

(A) UMAP plot showing clusters of mononuclear phagocyte subsets.

(B) Heatmap showing scaled expression of discriminative gene sets for mononuclear phagocyte subsets in OCT. The color scheme is based on *Z* score distribution from −2 (blue) to 2 (red).

(C–F) Volcano plots showing DEGs of CD16$^+$ Mos (C), CD14$^+$ Mos (D), DCs (E), and Macs (F) in TAO/HC comparison.

(G) The expression of CD36, CD163, and MRC1 by mononuclear phagocyte subsets from HCs and individuals with TAO patients by UMAP plot (left) and violin plot (right).

(H) Representative GO terms and KEGG pathway enriched by upregulated DEGs of Macs in OCT in TAO/HC comparison.

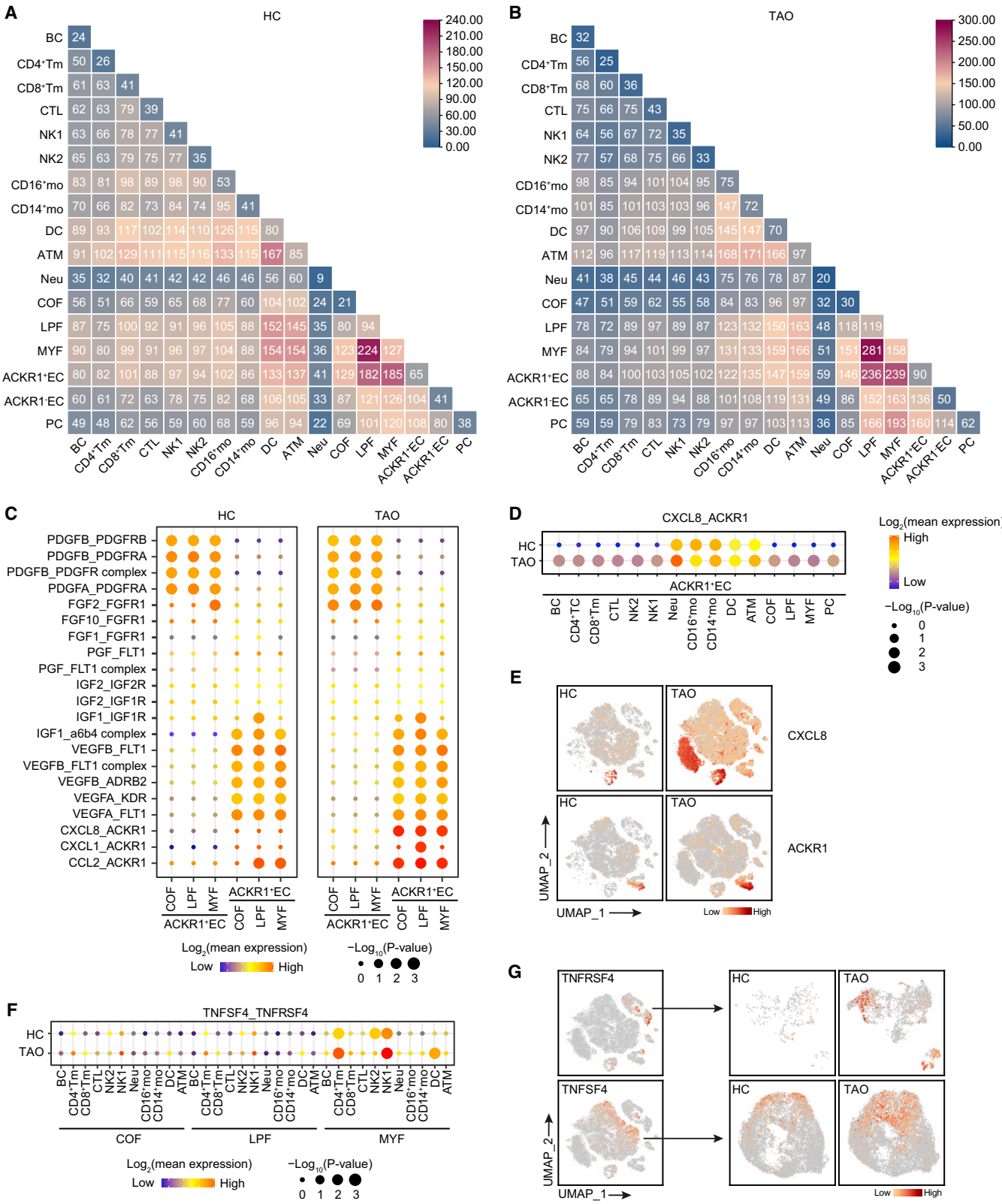

(legend on next page)

adipose tissue.[68] However, the role of ATMs in TAO has not yet been identified. In OCT, ACKR1$^+$ ECs expressed a high level of HIF1A, a critical molecule involved in hypoxia-induced angiogenesis.[69] Its downstream VEGF signaling is also upregulated in TAO, indicating that hypoxia may exist in the local environment of OCT. Our data showed that many cell types in OCT have a potent function in chemokine secretion. Thus, hypoxia and chemokines may also be two important factors for recruiting Mos/Macs in OCT in TAO. The ATMs identified in our study expressed M2 Mac markers but still retained pro-inflammatory signatures similar to the properties of ATMs from obese individuals.[70] These cells may actively engage in inflammation and lipid metabolism in the microenvironment of the OCT during TAO, as indicated by our transcriptional data.

Periocular tissue of individuals with TAO exhibited specific reactivity and characteristic remodeling.[6] We performed a high-dimensional single-cell analysis to obtain a comprehensive local cell landscape of TAO. This cell landscape depicted the compositional and functional alterations of cellular components of OCT in TAO and enriched our understanding of the pathogenic mechanisms underlying the TAO-characteristic changes in the orbital tissue. These informative transcriptional data can also act as a database for future exploration of TAO pathogenesis. Novel and specific treatments that directly target the pathogenic molecules or cells of TAO have long been sought. The results of this study indicate potential pathogenic cells and molecules, including LPFs with RASD expression, CD8$^+$CD57$^+$ CTLs, ATMs, ACKR1$^+$ ECs, and *Pim1*, which may account for the pathogenic changes of TAO, and, thus, may identify novel therapeutic targets for this disease.

We established a comprehensive transcriptional atlas of the local environment of OCT and revealed its changes during TAO at single-cell resolution. This study may expand our current knowledge of TAO and prompt the development of novel targeting therapies.

Limitations of the study

Although this study provides a good representation of the local circumstance of ocular connective tissues during TAO, some potential limitations should be noted. For example, limited by the availability of samples, our study only incorporated individuals with TAO who must undergo emergency decompression because of dysthyroid optic neuropathy. Individuals with mild illness or in the active disease phase without surgery indications or conditions were not involved in our study. Future studies should incorporate individuals with more diverse disease conditions, which allows comparisons of the length of the disease course, interventions (systemic steroid or radiotherapy), and even anatomical characteristics (dominated by extraocular fat expansion or muscle swelling). In addition, further experiments may enrich our study by evaluating these transcriptional changes with protein analysis in larger cohorts.

STAR★METHODS

Detailed methods are provided in the online version of this paper and include the following:

- KEY RESOURCES TABLE
- RESOURCE AVAILABILITY
  - Lead contact
  - Materials availability
  - Data and code availability
- EXPERIMENTAL MODEL AND SUBJECT DETAILS
  - Human orbital connective tissue
- METHOD DETAILS
  - Single-cell suspension preparation
  - scRNA sequencing
  - Raw data processing and quality control
  - Analysis of scRNA-seq data
  - Trajectory analysis
  - Cell–cell communication analysis with CellPhoneDB 2
  - Pathway analysis
  - Immunofluorescence staining
- QUANTIFICATION AND STATISTICAL ANALYSIS

SUPPLEMENTAL INFORMATION

Supplemental information can be found online at https://doi.org/10.1016/j.xcrm.2022.100699.

ACKNOWLEDGMENTS

This study was supported by the National Outstanding Youth Science Fund Project of China (8212200477).

AUTHOR CONTRIBUTIONS

X.W. and W.S. designed the study. M.W. and J.T. conducted the experiments and acquired samples. P.Z. and X.C. assisted with the experiments. Z.L. and L.Z. analyzed the scRNA-seq data. The manuscript was written by Z.L., L.Z., and R.D. and reviewed by all authors. Z.L., B.C., T.T., and R.W. prepared the figures and performed the statistical analyses. X.W. and W.S. verified the underlying data. All authors read and approved the final manuscript.

DECLARATION OF INTERESTS

The authors declare no competing interests.

Received: September 15, 2021
Revised: February 18, 2022
Accepted: July 8, 2022
Published: July 26, 2022

Figure 7. Development of an OF-based regulatory network for TAO

(A) Heatmap showing the interaction intensity among major cell subsets in OCT from HCs.
(B) Heatmap showing the interaction intensity among major cell subsets in OCT from TAO.
(C) The interaction of ACKR1$^+$ ECs with COFs, LPFs, and MYFs in individuals with TAO and HCs.
(D) The interaction of ACKR1$^+$ ECs with other major cell subsets in OCT from individuals with TAO and HCs via the CXCL8/ACKR1 interaction pair.
(E) UMAP plots showing the expression of CXCL8 and ACKR1 by OCT cells from HCs and individuals with TAO.
(F) The interaction of OF subsets with other major cell subsets in OCT from individuals with TAO and HCs via the TNFSF4/TNFRSF4 interaction pair.
(G) UMAP plots showing the expression of TNFRSF4 and TNFSF4 by OCT cells from HCs and individuals with TAO.

REFERENCES

1. Bahn, R.S. (2010). Graves' ophthalmopathy. N. Engl. J. Med. *362*, 726–738.
2. Salvi, M., Vannucchi, G., Currò, N., Campi, I., Covelli, D., Dazzi, D., Simonetta, S., Guastella, C., Pignataro, L., Avignone, S., and Beck-Peccoz, P. (2015). Efficacy of B-cell targeted therapy with rituximab in patients with active moderate to severe Graves' orbitopathy: a randomized controlled study. J. Clin. Endocrinol. Metab. *100*, 422–431.
3. Hamed Azzam, S., Kang, S., Salvi, M., and Ezra, D.G. (2018). Tocilizumab for thyroid eye disease. Cochrane Database Syst. Rev. *11*, CD012984.
4. Wiersinga, W.M. (2017). Advances in treatment of active, moderate-to-severe Graves' ophthalmopathy. The lancet. Lancet Diabetes Endocrinol. *5*, 134–142.
5. Taylor, P.N., Zhang, L., Lee, R.W.J., Muller, I., Ezra, D.G., Dayan, C.M., Kahaly, G.J., and Ludgate, M. (2020). New insights into the pathogenesis and nonsurgical management of Graves orbitopathy. Nat. Rev. Endocrinol. *16*, 104–116.
6. Łacheta, D., Miśkiewicz, P., Głuszko, A., Nowicka, G., Struga, M., Kantor, I., Pośledník, K.B., Mirza, S., and Szczepański, M.J. (2019). Immunological aspects of graves' ophthalmopathy. BioMed Res. Int. *2019*, 7453260.
7. Lehmann, G.M., Feldon, S.E., Smith, T.J., and Phipps, R.P. (2008). Immune mechanisms in thyroid eye disease. Thyroid *18*, 959–965.
8. Chen, M.H., Chen, M.H., Liao, S.L., Chang, T.C., and Chuang, L.M. (2008). Role of macrophage infiltration in the orbital fat of patients with Graves' ophthalmopathy. Clin. Endocrinol. *69*, 332–337.
9. Weetman, A.P., Cohen, S., Gatter, K.C., Fells, P., and Shine, B. (1989). Immunohistochemical analysis of the retrobulbar tissues in Graves' ophthalmopathy. Clin. Exp. Immunol. *75*, 222–227.
10. Hwang, C.J., Afifiyan, N., Sand, D., Naik, V., Said, J., Pollock, S.J., Chen, B., Phipps, R.P., Goldberg, R.A., Smith, T.J., and Douglas, R.S. (2009). Orbital fibroblasts from patients with thyroid-associated ophthalmopathy overexpress CD40: CD154 hyperinduces IL-6, IL-8, and MCP-1. Invest. Ophthalmol. Vis. Sci. *50*, 2262–2268.
11. Kuriyan, A.E., Woeller, C.F., O'Loughlin, C.W., Phipps, R.P., and Feldon, S.E. (2013). Orbital fibroblasts from thyroid eye disease patients differ in proliferative and adipogenic responses depending on disease subtype. Invest. Ophthalmol. Vis. Sci. *54*, 7370–7377.
12. van Zeijl, C.J., Fliers, E., van Koppen, C.J., Surovtseva, O.V., de Gooyer, M.E., Mourits, M.P., Wiersinga, W.M., Miltenburg, A.M., and Boelen, A. (2011). Thyrotropin receptor-stimulating Graves' disease immunoglobulins induce hyaluronan synthesis by differentiated orbital fibroblasts from patients with Graves' ophthalmopathy not only via cyclic adenosine monophosphate signaling pathways. Thyroid *21*, 169–176.
13. Fang, S., Huang, Y., Wang, N., Zhang, S., Zhong, S., Li, Y., Sun, J., Liu, X., Wang, Y., Gu, P., et al. (2019). Insights into local orbital immunity: evidence for the involvement of the th17 cell pathway in Thyroid-Associated ophthalmopathy. J. Clin. Endocrinol. Metab. *104*, 1697–1711.
14. Woeller, C.F., Roztocil, E., Hammond, C., and Feldon, S.E. (2019). TSHR signaling stimulates proliferation through PI3K/Akt and induction of miR-146a and miR-155 in thyroid eye disease orbital fibroblasts. Invest. Ophthalmol. Vis. Sci. *60*, 4336–4345.
15. West, M.D., Chang, C.F., Larocca, D., Li, J., Jiang, J., Sim, P., Labat, I., Chapman, K.B., Wong, K.E., Nicoll, J., et al. (2019). Clonal derivation of white and brown adipocyte progenitor cell lines from human pluripotent stem cells. Stem Cell Res. Ther. *10*, 7.
16. Prabhakar, B.S., Bahn, R.S., and Smith, T.J. (2003). Current perspective on the pathogenesis of Graves' disease and ophthalmopathy. Endocr. Rev. *24*, 802–835.
17. Sorisky, A., Pardasani, D., Gagnon, A., and Smith, T.J. (1996). Evidence of adipocyte differentiation in human orbital fibroblasts in primary culture. J. Clin. Endocrinol. Metab. *81*, 3428–3431.
18. Koumas, L., Smith, T.J., Feldon, S., Blumberg, N., and Phipps, R.P. (2003). Thy-1 expression in human fibroblast subsets defines myofibroblastic or lipofibroblastic phenotypes. Am. J. Pathol. *163*, 1291–1300.
19. Nie, X., Shen, C., Tan, J., Wu, Z., Wang, W., Chen, Y., Dai, Y., Yang, X., Ye, S., Chen, J., and Bian, J.S. (2020). Periostin: a potential therapeutic target for pulmonary hypertension? Circ. Res. *127*, 1138–1152.
20. Marusak, C., Thakur, V., Li, Y., Freitas, J.T., Zmina, P.M., Thakur, V.S., Chang, M., Gao, M., Tan, J., Xiao, M., et al. (2020). Targeting extracellular matrix remodeling restores BRAF inhibitor sensitivity in BRAFi-resistant melanoma. Clin. Cancer Res. *26*, 6039–6050.
21. Orr, S.K., Butler, K.L., Hayden, D., Tompkins, R.G., Serhan, C.N., and Irimia, D. (2015). Gene expression of proresolving lipid mediator pathways is associated with clinical outcomes in trauma patients. Crit. Care Med. *43*, 2642–2650.
22. Cha, J.Y., Kim, H.J., Yu, J.H., Xu, J., Kim, D., Paul, B.D., Choi, H., Kim, S., Lee, Y.J., Ho, G.P., et al. (2013). Dexras1 mediates glucocorticoid-associated adipogenesis and diet-induced obesity. Proc. Natl. Acad. Sci. USA *110*, 20575–20580.
23. Kim, H.J., Cha, J.Y., Seok, J.W., Choi, Y., Yoon, B.K., Choi, H., Yu, J.H., Song, S.J., Kim, A., Lee, H., et al. (2016). Dexras1 links glucocorticoids to insulin-like growth factor-1 signaling in adipogenesis. Sci. Rep. *6*, 28648.
24. Liu, Z., Han, M., Ding, K., and Fu, R. (2020). The role of Pim kinase in immunomodulation. Am. J. Cancer Res. *10*, 4085–4097.
25. Schildberg, F.A., and Donnenberg, V.S. (2018). Stromal cells in health and disease. Cytometry A. *93*, 871–875.
26. Ghesquière, B., Wong, B.W., Kuchnio, A., and Carmeliet, P. (2014). Metabolism of stromal and immune cells in health and disease. Nature *511*, 167–176.
27. Basha, G., Omilusik, K., Chavez-Steenbock, A., Reinicke, A.T., Lack, N., Choi, K.B., and Jefferies, W.A. (2012). A CD74-dependent MHC class I endolysosomal cross-presentation pathway. Nat. Immunol. *13*, 237–245.
28. Novitzky-Basso, I., and Rot, A. (2012). Duffy antigen receptor for chemokines and its involvement in patterning and control of inflammatory chemokines. Front. Immunol. *3*, 266.
29. Nibbs, R.J.B., and Graham, G.J. (2013). Immune regulation by atypical chemokine receptors. Nat. Rev. Immunol. *13*, 815–829.
30. Thiriot, A., Perdomo, C., Cheng, G., Novitzky-Basso, I., Mcardle, S., Kishimoto, J.K., Barreiro, O., Mazo, I., Triboulet, R., Ley, K., et al. (2017). Differential DARC/ACKR1 expression distinguishes venular from non-venular endothelial cells in murine tissues. BMC Biol. *15*, 45.
31. Wang, G.L., Jiang, B.H., Rue, E.A., and Semenza, G.L. (1995). Hypoxia-inducible factor 1 is a basic-helix-loop-helix-PAS heterodimer regulated by cellular O2 tension. Proc. Natl. Acad. Sci. USA *92*, 5510–5514.
32. Han, R., and Smith, T.J. (2006). T helper type 1 and type 2 cytokines exert divergent influence on the induction of prostaglandin E2 and hyaluronan synthesis by interleukin-1beta in orbital fibroblasts: implications for the pathogenesis of thyroid-associated ophthalmopathy. Endocrinology *147*, 13–19.
33. Bednarczuk, T., Hiromatsu, Y., Inoue, Y., Yamamoto, K., Wall, J.R., and Nauman, J. (2002). T-cell-mediated immunity in thyroid-associated ophthalmopathy. Thyroid *12*, 209–215.
34. Blackburn, S.D., Shin, H., Haining, W.N., Zou, T., Workman, C.J., Polley, A., Betts, M.R., Freeman, G.J., Vignali, D.A.A., and Wherry, E.J. (2009). Coregulation of CD8+ T cell exhaustion by multiple inhibitory receptors during chronic viral infection. Nat. Immunol. *10*, 29–37.
35. Kared, H., Martelli, S., Ng, T.P., Pender, S.L.F., and Larbi, A. (2016). CD57 in human natural killer cells and T-lymphocytes. Cancer Immunol. Immunother. *65*, 441–452.
36. Ouyang, Q., Wagner, W.M., Voehringer, D., Wikby, A., Klatt, T., Walter, S., Müller, C.A., Pircher, H., and Pawelec, G. (2003). Age-associated accumulation of CMV-specific CD8+ T cells expressing the inhibitory killer cell lectin-like receptor G1 (KLRG1). Exp. Gerontol. *38*, 911–920.

37. Rosen, C.E., Rizzuto, P.R., Kennerdell, J.S., Burde, R.M., and Wall, J.R. (1994 Oct-Dec). Interleukin-2 receptor beta and CD57 expression in orbital tissues from patients with chronic, stable thyroid-associated ophthalmopathy. Alaska Med. *36*, 177–182. 207.

38. Le Priol, Y., Puthier, D., Lécureuil, C., Combadière, C., Debré, P., Nguyen, C., and Combadière, B. (2006). High cytotoxic and specific migratory potencies of senescent CD8+ CD57+ cells in HIV-infected and uninfected individuals. J. Immunol. *177*, 5145–5154.

39. Narasimhan, P.B., Marcovecchio, P., Hamers, A.A.J., and Hedrick, C.C. (2019). Nonclassical monocytes in health and disease. Annu. Rev. Immunol. *37*, 439–456.

40. Snelgrove, R.J., Goulding, J., Didierlaurent, A.M., Lyonga, D., Vekaria, S., Edwards, L., Gwyer, E., Sedgwick, J.D., Barclay, A.N., and Hussell, T. (2008). A critical function for CD200 in lung immune homeostasis and the severity of influenza infection. Nat. Immunol. *9*, 1074–1083.

41. Lumeng, C.N., Bodzin, J.L., and Saltiel, A.R. (2007). Obesity induces a phenotypic switch in adipose tissue macrophage polarization. J. Clin. Invest. *117*, 175–184.

42. Silverstein, R.L., and Febbraio, M. (2009). CD36, a scavenger receptor involved in immunity, metabolism, angiogenesis, and behavior. Sci. Signal. *2*, re3.

43. Trombetta, A.C., Soldano, S., Contini, P., Tomatis, V., Ruaro, B., Paolino, S., Brizzolara, R., Montagna, P., Sulli, A., Pizzorni, C., et al. (2018). A circulating cell population showing both M1 and M2 monocyte/macrophage surface markers characterizes systemic sclerosis patients with lung involvement. Respir. Res. *19*, 186.

44. Wang, Y., and Smith, T.J. (2014). Current concepts in the molecular pathogenesis of thyroid-associated ophthalmopathy. Invest. Ophthalmol. Vis. Sci. *55*, 1735–1748.

45. Antonelli, A., Ferrari, S.M., Fallahi, P., Frascerra, S., Santini, E., Franceschini, S.S., and Ferrannini, E. (2009). Monokine induced by interferon gamma (IFNgamma) (CXCL9) and IFNgamma inducible T-cell alpha-chemoattractant (CXCL11) involvement in Graves' disease and ophthalmopathy: modulation by peroxisome proliferator-activated receptor-gamma agonists. J. Clin. Endocrinol. Metab. *94*, 1803–1809.

46. Reynolds, G., Vegh, P., Fletcher, J., Poyner, E.F.M., Stephenson, E., Goh, I., Botting, R.A., Huang, N., Olabi, B., Dubois, A., et al. (2021). Developmental cell programs are co-opted in inflammatory skin disease. Science *371*, eaba6500.

47. Webb, G.J., Hirschfield, G.M., and Lane, P.J.L. (2016). OX40, OX40L and autoimmunity: a comprehensive review. Clin. Rev. Allergy Immunol. *50*, 312–332.

48. Ishii, N., Takahashi, T., Soroosh, P., and Sugamura, K. (2010). OX40-OX40 ligand interaction in T-cell-mediated immunity and immunopathology. Adv. Immunol. *105*, 63–98.

49. Elhai, M., Avouac, J., Hoffmann-Vold, A.M., Ruzehaji, N., Amiar, O., Ruiz, B., Brahiti, H., Ponsoye, M., Fréchet, M., Burgevin, A., et al. (2016). OX40L blockade protects against inflammation-driven fibrosis. Proc. Natl. Acad. Sci. USA *113*, E3901–E3910.

50. Paik, D.T., Cho, S., Tian, L., Chang, H.Y., and Wu, J.C. (2020). Single-cell RNA sequencing in cardiovascular development, disease and medicine. Nat. Rev. Cardiol. *17*, 457–473.

51. Wilk, A.J., Rustagi, A., Zhao, N.Q., Roque, J., Martínez-Colón, G.J., Mckechnie, J.L., Ivison, G.T., Ranganath, T., Vergara, R., Hollis, T., et al. (2020). A single-cell atlas of the peripheral immune response in patients with severe COVID-19. Nat. Med. *26*, 1070–1076.

52. Smith, T.J., Koumas, L., Gagnon, A., Bell, A., Sempowski, G.D., Phipps, R.P., and Sorisky, A. (2002). Orbital fibroblast heterogeneity may determine the clinical presentation of thyroid-associated ophthalmopathy. J. Clin. Endocrinol. Metab. *87*, 385–392.

53. Zemskova, M.Y., Song, J.H., Cen, B., Cerda-Infante, J., Montecinos, V.P., and Kraft, A.S. (2015). Regulation of prostate stromal fibroblasts by the PIM1 protein kinase. Cell. Signal. *27*, 135–146.

54. Nga, M.E., Swe, N.N.M., Chen, K.T., Shen, L., Lilly, M.B., Chan, S.P., Salto-Tellez, M., and Das, K. (2010). PIM-1 kinase expression in adipocytic neoplasms: diagnostic and biological implications. Int. J. Exp. Pathol. *91*, 34–43.

55. Pober, J.S., and Sessa, W.C. (2007). Evolving functions of endothelial cells in inflammation. Nat. Rev. Immunol. *7*, 803–815.

56. Halin, C., Mora, J.R., Sumen, C., and von Andrian, U.H. (2005). In vivo imaging of lymphocyte trafficking. Annu. Rev. Cell Dev. Biol. *21*, 581–603.

57. Ley, K., and Reutershan, J. (2006). Leucocyte-endothelial interactions in health and disease. Handb. Exp. Pharmacol., 97–133.

58. Huang, Y., Fang, S., Li, D., Zhou, H., Li, B., and Fan, X. (2019). The involvement of T cell pathogenesis in thyroid-associated ophthalmopathy. Eye *33*, 176–182.

59. Wakelkamp, I.M.M.J., Bakker, O., Baldeschi, L., Wiersinga, W.M., and Prummel, M.F. (2003). TSH-R expression and cytokine profile in orbital tissue of active vs. Inactive Graves' ophthalmopathy patients. Clin. Endocrinol. *58*, 280–287.

60. Mikoś, H., Mikoś, M., Obara-Moszyńska, M., and Niedziela, M. (2014). The role of the immune system and cytokines involved in the pathogenesis of autoimmune thyroid disease (AITD). Endokrynol. Pol. *65*, 150–155.

61. Nishimura, S., Manabe, I., Nagasaki, M., Eto, K., Yamashita, H., Ohsugi, M., Otsu, M., Hara, K., Ueki, K., Sugiura, S., et al. (2009). CD8+ effector T cells contribute to macrophage recruitment and adipose tissue inflammation in obesity. Nat. Med. *15*, 914–920.

62. Brenchley, J.M., Karandikar, N.J., Betts, M.R., Ambrozak, D.R., Hill, B.J., Crotty, L.E., Casazza, J.P., Kuruppu, J., Migueles, S.A., Connors, M., et al. (2003). Expression of CD57 defines replicative senescence and antigen-induced apoptotic death of CD8+ T cells. Blood *101*, 2711–2720.

63. Wang, Y., Chen, Z., Wang, T., Guo, H., Liu, Y., Dang, N., Hu, S., Wu, L., Zhang, C., Ye, K., and Shi, B. (2021). A novel CD4+ CTL subtype characterized by chemotaxis and inflammation is involved in the pathogenesis of Graves' orbitopathy. Cell. Mol. Immunol. *18*, 735–745.

64. Chattopadhyay, P.K., Betts, M.R., Price, D.A., Gostick, E., Horton, H., Roederer, M., and De Rosa, S.C. (2009). The cytolytic enzymes granyzme a, granzyme B, and perforin: expression patterns, cell distribution, and their relationship to cell maturity and bright CD57 expression. J. Leukoc. Biol. *85*, 88–97.

65. Yi, J.S., Cox, M.A., and Zajac, A.J. (2010). T-cell exhaustion: characteristics, causes and conversion. Immunology *129*, 474–481.

66. Akbar, A.N., and Henson, S.M. (2011). Are senescence and exhaustion intertwined or unrelated processes that compromise immunity? Nat. Rev. Immunol. *11*, 289–295.

67. Hill, D.A., Lim, H.W., Kim, Y.H., Ho, W.Y., Foong, Y.H., Nelson, V.L., Nguyen, H.C.B., Chegireddy, K., Kim, J., Habertheuer, A., et al. (2018). Distinct macrophage populations direct inflammatory versus physiological changes in adipose tissue. Proc. Natl. Acad. Sci. USA *115*, E5096–E5105.

68. Sun, K., Kusminski, C.M., and Scherer, P.E. (2011). Adipose tissue remodeling and obesity. J. Clin. Invest. *121*, 2094–2101.

69. Pugh, C.W., and Ratcliffe, P.J. (2003). Regulation of angiogenesis by hypoxia: role of the HIF system. Nat. Med. *9*, 677–684.

70. Zeyda, M., Farmer, D., Todoric, J., Aszmann, O., Speiser, M., Györi, G., Zlabinger, G.J., and Stulnig, T.M. (2007). Human adipose tissue macrophages are of an anti-inflammatory phenotype but capable of excessive pro-inflammatory mediator production. Int. J. Obes. *31*, 1420–1428.

71. Butler, A., Hoffman, P., Smibert, P., Papalexi, E., and Satija, R. (2018). Integrating single-cell transcriptomic data across different conditions, technologies, and species. Nat. Biotechnol. *36*, 411–420.

72. Korsunsky, I., Millard, N., Fan, J., Slowikowski, K., Zhang, F., Wei, K., Baglaenko, Y., Brenner, M., Loh, P.R., and Raychaudhuri, S. (2019). Fast, sensitive and accurate integration of single-cell data with Harmony. Nat. Methods *16*, 1289–1296.

73. Qiu, X., Mao, Q., Tang, Y., Wang, L., Chawla, R., Pliner, H.A., and Trapnell, C. (2017). Reversed graph embedding resolves complex single-cell trajectories. Nat. Methods *14*, 979–982.

74. Vento-Tormo, R., Efremova, M., Botting, R.A., Turco, M.Y., Vento-Tormo, M., Meyer, K.B., Park, J.E., Stephenson, E., Polański, K., Goncalves, A., et al. (2018). Single-cell reconstruction of the early maternal-fetal interface in humans. Nature *563*, 347–353.

75. Zhou, Y., Zhou, B., Pache, L., Chang, M., Khodabakhshi, A.H., Tanaseichuk, O., Benner, C., and Chanda, S.K. (2019). Metascape provides a biologist-oriented resource for the analysis of systems-level datasets. Nat. Commun. *10*, 1523.

76. Ginestet, C. (2011). Ggplot2: elegant graphics for data analysis. J. Roy. Stat. Soc. *174*, 245–246.

STAR★METHODS

KEY RESOURCES TABLE

REAGENT or RESOURCE	SOURCE	IDENTIFIER
Antibodies		
PIM1 Antibody (ST0513)	NOVUS	Cat# NBP2-67528
Biological samples		
Obital connective tissue from TAO patient	Sun Yat-sen Memorial Hospital and Xiangya Hospital	See Table S1 for details
Obital connective tissue from healthy donors	Zhongshan Ophthalmic Center	See Table S1 for details
Chemicals, peptides, and recombinant proteins		
DMEM/F-12 (1:1) basic (1X)	GIBCO	LOT# 8119025
Fetal Bovine Serum (FBS), qualified, Australia	GIBCO	Cat# 10099141C
Collagenase II	GIBCO	Cat#17101-015
DNase I	Sigma-Aldrich	Cat#DN25
Phosphate Buffer Saline (PBS, 1X)	CORNING	LOT# 21020007
Tissue-Tek O.C.T Compound	Sakura Finetek USA, Inc	LOT# 0565-00
Critical commercial assays		
Chromium Single Cell 3′ Library & Gel Bead Kit v2	10X Genomics	Cat#PN-120237
Deposited data		
Raw data files files for scRNA-seq	This study	GSA: HRA000870
Software and algorithms		
Cell Ranger (version: 5.0.0)	10x Genomics	https://support.10xgenomics.com/single-cell-gene-expression/software/downloads/latest
Loupe Browser (version: 5.0.0)	10x Genomics	https://support.10xgenomics.com/single-cell-gene-expression/software/downloads/latest
R (version: 4.3.0)	R Core	https://www.r-project.org/
Seurat (version: 4.0.1)	Butler et al., 2018	https://satijalab.org/seurat/
Harmony (version 2.0.4)	Korsunsky et al., 2019	https://github.com/pardeike/Harmony
Metascape (version: 3.5)	Zhou et al., 2019	http://metascape.org/
Monocle (version: 2.99.3)	Qiu et al., 2017	http://cole-trapnell-lab.github.io/monocle-release/docs/
CellPhoneDB 2	Github	https://github.com/ventolab/CellphoneDB
pheatmap (version: 1.0.12)	N/A	https://cran.r-project.org/web/packages/pheatmap/index.html
ggplot2 (version: 3.2.1)	Wickham, 2016	https://ggplot2.tidyverse.org/
ImageJ (version: 1.8.0)	NIH	https://imagej.nih.gov/ij/
GraphPad Prism 8	GraphPad Software Inc.	https://www.graphpad.com/scientific-software/prism/

RESOURCE AVAILABILITY

Lead contact

Further information and requests for resources and reagents should be directed to and will be fulfilled by the lead contact, Wenru Su (suwr3@mail.sysu.edu.cn).

Materials availability

This study did not generate new unique reagents.

Data and code availability

The single-cell data supporting the findings of this study including raw.fcs files from primary samples and cell lines have been deposited at Genome Sequence Archive (GSA) and are publicly available as of the date of publication (GSA: HRA000870).

The data analysis pipeline in our study was described on the Seurat websites: https://satijalab.org/seurat/. The Monocle package and related code can be found at: http://cole-trapnell-lab.github.io/monocle-release/docs/. The CellPhoneDB package and related code is available at Github: https://github.com/ventolab/CellphoneDB.

Any additional information required to reanalyze the data reported in this work paper is available from the lead contact upon request.

EXPERIMENTAL MODEL AND SUBJECT DETAILS

Human orbital connective tissue

Twenty retroorbital connective tissue samples were included in the study. Ten samples were from patients with TAO who underwent orbital decompression surgery and with a clinical activity score of >3. The other ten samples were from healthy participants who underwent blepharoplasty. Steroid or immunosuppressive treatment was discontinued for at least 3 months before surgery, and all patients were clinically euthyroid at the time of surgery. The clinical characteristic of these patients is shown in Table S1. Samples were obtained from the Zhongshan Ophthalmic Center, Sun Yat-Sen University, Guangzhou, China; Sun Yat-sen Memorial Hospital, Sun Yat-sen University, Guangzhou, China and Xiangya Hospital, Central South University, Changsha, China. Informed consent was obtained from all the participants. All experimental procedures were approved by the Ethical Committee of Zhongshan Ophthalmic Center, Sun Yat-Sen University, Guangzhou, China (2020KYPJ104), and Sun Yat-sen Memorial Hospital, Sun Yat-sen University, Guangzhou, China (2020-KY-122).

METHOD DETAILS

Single-cell suspension preparation

Orbital connective tissues were processed immediately after being obtained. Every sample was cut into small pieces (<1 mm in diameter) and then was incubated with DMEM (Thermo Fisher Scientific) containing 2% FBS (Thermo Fisher Scientific), 1 mg/mL of Collagenase II (Sigma-Aldrich), and 100 μL of DNase I (Sigma-Aldrich) for 1 h on a 37°C shaker. Subsequently, 4 mL DMEM was added to dilute the suspension, and then a 70-μm cell mesh was used to filter the suspension. After centrifugation at 300*g* and 4°C for 10 min, the supernatant was discarded, and then the cells were washed with PBS twice. Then, the cell pellet was resuspended in 10 mL of ice-cold red blood cell lysis buffer and was incubated at 4°C for 15 min. Next, 10 mL of ice-cold PBS was added to the tube, and it was then centrifuged at 250 g for 10 min. After the supernatant was decanted, the pellet was resuspended in 5 mL of calcium- and magnesium-free PBS containing 0.04% weight/volume BSA. The single-cell suspension was generated at 700–1200/uL (viability $\geq$85%) as determined using the Countess II Automated Cell Counter. Each HC group (HC1, HC2) included five healthy participants' samples. TAO2 and TAO3 included three TAO patients' samples, while TAO1 and TAO4 included two TAO patients' samples.

scRNA sequencing

According to the manufacturer's protocol, Chromium Single Cell 3′ Reagent v2 kits (10X Genomics) were used to prepare barcoded single-cell RNA sequencing (scRNA-seq) libraries. Single-cell suspensions were loaded onto a chromium single-cell controller instrument (10X Genomics) to generate single-cell gel beads in emulsions. Approximately 12,000 cells were added to each channel to capture 8,000 cells per library. First, reverse transcription reactions were performed to generate barcoded full-length cDNA, followed by disruption of emulsions using the recovery agent and then cDNA clean-up using DynaBeads Myone Silane Beads (Thermo Fisher Scientific). Next, cDNA was amplified through polymerase chain reaction for the appropriate number of cycles depending on the number of recovered cells. Subsequently, the amplified cDNA was fragmented, nd-repaired, A-tailed, and ligated to an index adaptor, after which the library was amplified. Each library was sequenced on a NovaSeq platform (Illumina), and 150 bp paired-end reads were generated.

Raw data processing and quality control

The single-cell suspension was generated at 700–1200/ul (viability $\geq$85%) as determined using the Countess® II Automated Cell Counter. Raw data (Raw Reads) of FASTQ files were transformed from the Raw BCL files using Illumina's bcl2fastq converter and for Raw data, firstly processed through primary quality control. Reads were removed out of the downstream analysis when they meet one of the following three conditions: (1) contain N base more than 3; (2) with more than 20% bases with Phred <5; (3) have adapter sequences. All the downstream analyses were based on clean data with high quality.

Analysis of scRNA-seq data

CellRanger version 5.0.0 (10X Genomics) function ''cellranger count'' was used to process the raw data, demultiplex cellular barcodes, and map reads to the human reference genome GRCh38-2020 (10X Genomics). Then ''cellranger aggr'' function was used to generate normalized aggregate data across samples. ''cellranger aggr'' function aggregates outputs from multiple runs of cellranger count, normalizing those runs to the same sequencing depth and then recomputing the feature-barcode matrices and analysis on the combined data. The aggr pipeline can be used to combine data from multiple samples into an experiment-wide feature-barcode matrix and analysis. These processes produced a raw unique molecular identifier count matrix that was converted into a Seurat object using the R package Seurat[71] (version 4.0.1, https://github.com/satijalab/seurat). Quality control was done to ensure that the percentage of mitochondrial transcripts was smaller than 15% and the identified gene number in each cell ranged from 200 to 6000 for elimination of potential cell debris or doublets. Finally, 31,353 cells remained and were used in downstream analyses. After quality control filtering, Seurat packages were used to performed log normalization on the UMI count matrix. In addition, the samples were scaled. Samples were processed and sequenced in batches. The Harmony (version 2.0.4, https://github.com/pardeike/Harmony) algorithm[72] was used for batch effect correction. We performed dimension reduction clustering and differential expression analysis following the Seurat-guided tutorial. We performed principal component analysis (PCA) and uniform manifold approximation and projection (UMAP) dimension reduction with 20 principal components. The main cell clusters were identified using the ''FindClusters()'' function, with the resolution set as default (res = 0.5). They were then visualized using t-distributed stochastic neighbor embedding (tSNE) or uniform manifold approximation and projection (UMAP) plots. Conventional markers described in a previous study were used to categorize every cell into a known biological cell type. The ''FindAllMarker()'' function was used to identify preferentially expressed genes in clusters or differentially expressed genes between cells from patients with TAO and HCs.

Trajectory analysis

Pseudotime analysis was performed with Monocle2[73] to determine the translational relationships among monocyte-derived cells and clusters. Further detection using the Monocle2 ''plot_pseudotime_heatmap'' function revealed the key role of a series of genes in the differentiation process. Genes with significant changes were identified through the ''differentialGeneTest'' function in Monocle2 with a q-value < 0.01.

Cell–cell communication analysis with CellPhoneDB 2

CellPhoneDB 2[74] is a Python-based computational analysis tool developed by Roser Vento-Tormo et al. for the molecular analysis of cell–cell communication. It was used in this study to determine interaction networks. A website version is available for the analysis of a relatively small dataset (http://www.cellphonedb.org/). There were 31,353 single cells (10517 HC and 20836 TAO) clustered into 18 cell types. Interaction pairs whose ligands belonged to the VEGF, FGF, PDGF, PGF, IGF, CCL, or CXCL and so on. families and had p-values < 0.05 were selected for the evaluation of relationships between cell types.

Pathway analysis

DE-Gs of the cell subtypes were identified using the ''FindMarker()'' function of Seurat. The cut-off criteria were |FC| > 0.25 and adj.p.val <0.05. Enrichment analysis was performed on these DE-Gs using the Matascape[75] webtool (https://metascape.org/gp/index.html). GO terms and the Kyoto Encyclopedia of Genes and Genomes (KEGG) pathways were used in this study. The FDR was calculated using the Benjamini–Hochberg procedure and used as the metric for GO terms in order to account for multiple testing. Among the top 100 enriched GO terms across different cell types, five to ten GO terms or pathways that were associated with EAU were graphed with the heatmap (version 1.0.12) and ggplot2 package.[76]

Immunofluorescence staining

Orbital connective tissues were removed and fixed with 4% paraformaldehyde overnight at 4 °C, dehydrated using sucrose with different concentration gradients (10%, overnight; 20%, 6–8 h; 30%, overnight) and embedded in Tissue-Tek O.C.T Compound (Sakura Finetek USA, Inc). Sagittal sections (4-μm thick) were cut and blocked with 3% BSA in PBS for 1 h at 23°C ± 2°C. The sections were incubated with *PIM1* Antibody (ST0513, NOVUS, Cat# NBP2-67528) overnight at 4°C and further incubated with the corresponding fluorochrome-conjugated secondary antibody (1:1,000, Cell Signaling Technology, Danvers, MA, USA) for 50 min. After counterstaining with DAPI (catalog ab104139, Abcam), the sections were examined with a fluorescence microscope (Nikon, Tokyo, Japan). The proportion of immunoreactive cells was analyzed via ImageJ software.

QUANTIFICATION AND STATISTICAL ANALYSIS

The Seurat function ''FindMarkers()'' was used to compare expression values. Cell type markers were obtained using the ''FindAllMarkers()'' function with a negative binomial test. All statistical analyses and graphs were done using R (version 4.3.0) and GraphPad Prism (version 8.0.2). Adjusted p-values above 0.05 were considered as not significant. Benjamini–Hochberg false discovery rate (FDR) correction was performed at a p-value of 0.05 for multiple comparison correction (proportions for subtypes of scRNA data).